Eurasian Chem.-Technol. J. 27 (2025) 13–20
The journal of the Institute of Combustion Problems https://ect-journal.kz

https://doi.org/10.18321/ectj1652

Nano- and Micro-Sized $LaNi_5$ Electrochemical Behaviour as Anode Material for Ni-MH Batteries

S.D. Malik[1], Ya.S. Zhigalenok[1], M.K. Skakov[2], A.Zh. Miniyazov[3], N.M. Mukhamedova[3], F.I. Malchik[1]*

[1]Center of Physical-Chemical Methods of Research and Analysis, al-Farabi Kazakh National University, 96A, Tole bi str., Almaty, Kazakhstan
[2]National Nuclear Center of the Republic of Kazakhstan, 180010, 2B, Beibyt atom str., Kurchatov, Kazakhstan
[3]Institute of Atomic Energy of National Nuclear Center of the Republic of Kazakhstan, 180010, 2B, Beibyt atom str., Kurchatov, Kazakhstan

Article info

Received:
5 November 2024

Received in revised form:
26 December 2024

Accepted:
2 February 2025

Keywords:
Hydrogen storage
Ni-MH batteries
Anode material
$LaNi_5$
Nanoparticles

ABSTRACT

This study investigates the electrochemical characteristics of nanostructured $LaNi_5$ intermetallic synthesized via the sol-gel method for application as an anode material in nickel-metal hydride (Ni-MH) batteries. A comparison with a commercial counterpart produced by fusion synthesis with mechanical grinding revealed that the nanostructured material, with primary particle sizes of 300–700 nm, exhibits significantly improved kinetic properties, including reduced charge transfer resistance and more efficient mass transport. The synthesized $LaNi_5$ demonstrates rapid activation, reaching a maximum capacity of 180 mAh/g by the 5^{th} cycle, although degradation to 130 mAh/g is observed by the 50^{th} cycle. In contrast, the commercial sample exhibits slow activation, with a gradual capacity increase to 190 mAh/g followed by stabilization. This discrepancy between enhanced kinetic properties and cycle stability in the nanostructured material presents a promising direction for optimizing anode materials in Ni-MH batteries.

1. Introduction

Nickel-metal hydride (Ni-MH) batteries are widely used in portable electronics and electric vehicles due to their combination of high specific energy, stable operation across a broad temperature range, environmental safety, and recyclability [1–3]. The anode plays a crucial role in such systems, requiring efficient and reversible hydrogen storage. The most common anode materials are AB_5-type intermetallic alloys, with $LaNi_5$ being one of the most extensively studied representatives of this family [4]. Under full hydrogenation ($LaNi_5H_6$), a theoretical specific capacity of approximately 372 mAh/g can be achieved. However, under real conditions, where the partial pressure of hydrogen is close to atmospheric, practical capacities of only 150–200 mAh/g are attained, corresponding to $LaNi_5H_x$ hydrides (x = 2.4–3.2) [5,6]. This discrepancy between theoretical and practical values is attributed to thermodynamic and kinetic factors influencing hydrogen absorption, as well as technological aspects related to powder preparation.

The most established method for synthesizing $LaNi_5$ involves high-temperature melting (arc [7] or induction [8]) in an inert atmosphere at temperatures exceeding 2000 °C, followed by mechanical grinding of the resulting ingot [9]. While this method ensures precise control over the chemical composition and phase purity of the alloy, achieving fine particle fractions requires prolonged grinding, leading to high energy consumption and difficulties in obtaining submicron particles [10]. Extended mechan-

*Corresponding author.
E-mail address: frodo-007@mail.ru

ical grinding can reduce particle sizes to the micron range (20–100 μm), with occasional fractions reaching as small as 500 nm [11]. However, such extensive grinding often results in a high concentration of defects. The excessive defect density caused by impact and friction can degrade the hydrogen absorption properties [12,13].

An alternative approach is mechanical alloying, where La and Ni powders (or their compounds) are co-milled in planetary mills, inducing local heating and reactive interactions without the need for high-temperature melting [11]. However, this method also requires considerable energy input and does not always ensure uniform nanostructuring without unwanted phase transformations.

The challenge lies in the fact that the particle size of $LaNi_5$ directly determines the efficiency of electrochemical processes in Ni-MH batteries: as the size decreases, the specific surface area and electrolyte contact increase, and as a result, diffusion limitations during charge-discharge cycles diminish [14]. However, forced grinding of the initial coarse-grained alloy leads to defect accumulation, which can negatively impact performance [15]. Another issue is $LaNi_5$ degradation during cycling: by the 100^{th}–200^{th} cycle, capacity decreases by 30–40%, attributed to intermetallic disproportionation (formation of LaH_3 and metallic nickel) [16], as well as irreversible structural changes during repeated hydrogen absorption and desorption cycles [17]. Moreover, particles of varying degrees of fragmentation degrade unevenly, lose electrical contact, and accelerate anode deterioration. These factors highlight the potential of synthesizing $LaNi_5$ directly in submicron or nanocrystalline form, avoiding prolonged and energy-intensive grinding and minimizing associated structural defects.

One method for producing dispersed powders is gas atomization or spray drying of molten metal: droplets rapidly cool in a gas flow, forming spherical particles of the desired size. For instance, Lui et al. reported a gas-phase synthesis of $LaNi_5$ particles measuring 28–58 nm [18]. However, gas-phase methods often result in low yields, and gas atomization equipment is expensive and technologically complex.

Consequently, increasing attention is being given to chemical synthesis methods based on low-temperature exothermic reactions, which allow direct synthesis of nanostructured powder [19]. For example, Yasuda et al. [20] synthesized $LaNi_5$ by heating a mixture of La_2O_3, Ni, and Ca in a hydrogen atmosphere, where calcium reacts with H_2 to form CaH_2, releasing significant heat. This exothermic reaction provides the energy necessary for La_2O_3 reduction to metallic lanthanum, followed by intermetallic synthesis, yielding particles of 5–10 μm. The resulting material exhibited a hydrogen sorption capacity of 1.31 wt.% H_2 (theoretical: 1.4 wt.% [21]), confirming the method's effectiveness. Burlakova et al. [22] employed the reduction of $La_2Ni_{10}(CO_3)_8(OH)_{10}\times54H_2O$ carbonate precursors using CaH_2, obtaining particles around 200 nm at temperatures up to 1000 °C.

Liu et al. [23] applied the sol-gel method, utilizing exothermic reactions between metal salts and an organic reducing agent (glycine), leading to oxide formation, which was subsequently reduced at ~600 °C to $LaNi_5$ with particle sizes of approximately 170 nm. The resulting powder exhibited a hydrogen sorption capacity of about 1.0 wt.% and demonstrated improved kinetics, with complete hydrogen desorption in less than 5 min at 0.05 MPa pressure. However, over time, a decline in sorption capacity was observed, which the authors attributed to the high number of grain boundaries promoting structural defect accumulation.

During gas-phase hydrogen absorption, characterized by rapid kinetic processes, molecular hydrogen dissociates at active surface sites and diffuses into the crystal lattice. Local atomic hydrogen accumulation near defect zones can lead to hydride phase formation with increased hydrogen concentration. This process may cause structural instability due to internal stresses, phase transitions, and potential material degradation. In contrast, electrochemical hydrogen sorption occurs at lower rates, enabling gradual atomic hydrogen intercalation into the crystal lattice. This reduces the probability of localized overstress and facilitates structural relaxation. Presumably, the more controlled hydrogen uptake during electrochemical intercalation could mitigate defects through their redistribution and possible lattice restructuring.

Therefore, this study investigates $LaNi_5$ synthesized via the sol-gel method, aiming to leverage the potential kinetic benefits of nanostructuring for Ni-MH battery anodes. Critically, and representing the primary advantage over many previous works, we conduct a direct and detailed electrochemical comparison between this synthesized nano-$LaNi_5$ and a standard commercial microcrystalline sample. This involves analyzing reaction kinetics through cyclic voltammetry and impedance spectroscopy, alongside evaluating long-term cycling stability via galvanostatic charge-discharge tests. Such a direct comparison is essential for understanding the

practical trade-offs between enhanced kinetics and cycling durability associated with using sol-gel derived nanostructured $LaNi_5$ as an anode material, revealing faster kinetics but lower stability for the nanostructured form in contrast to the commercial counterpart.

2. Experimental section

2.1 Materials

Nickel nitrate hexahydrate ($Ni(NO_3)_2{\times}6H_2O$, ≥99.9%), lithium chloride (LiCl, 99.0%), lanthanum nitrate hexahydrate ($La(NO_3)_3{\times}6H_2O$, ≥99.9%), lanthanum-nickel alloy ($LaNi_5$, ≥99.5%), calcium hydride (CaH_2) (99%) and a 60% aqueous emulsion of polytetrafluoroethylene (PTFE) were purchased from Sigma-Aldrich (USA). Ammonium chloride (NH_4Cl) (≥99.5%) was obtained from Reachem (Russia). All chemicals were used without further purification.

2.2 Synthesis of $LaNi_5$

The two-stage synthesis of the $LaNi_5$ intermetallic was carried out according to the methodology described in [23], with an optimized washing procedure. In the original method, washing the synthesized product to remove CaO was performed with a 0.11 M NH_4Cl solution in absolute ethanol, which resulted in the formation of $CaCl_2$ and the release of NH_3. However, due to the low solubility of NH_4Cl in absolute ethanol (0.6 g per 100 g at 20 °C), the efficiency of CaO removal was limited. In the present method, treatment was conducted in air using an aqueous 4 M NH_4Cl solution. This significantly improved CaO removal efficiency due to the high solubility of NH_4Cl in water (up to 37.2 g per 100 g at 20 °C), ensuring a sufficient reagent concentration. After washing, the purified product was dried at 80–100 °C under vacuum.

2.3 Grinding of Commercial $LaNi_5$

The large particles of commercial $LaNi_5$ (~100 μm, Sigma-Aldrich) were unsuitable for electrode fabrication, necessitating mechanical grinding in a planetary ball mill. Wet milling was performed using zirconia oxide balls at a ball-to-material mass ratio of 6:1 for 4 h at a rotation speed of 400 rpm. Ethanol was used as a solvent due to its low boiling point (78.4 °C), which reduced drying time and prevented particle agglomeration. After homogenization, the material was dried in a vacuum oven at 200 °C for 4 hours.

2.4 Fabrication of $LaNi_5$ Electrode Material

A 300 ml agate mortar was loaded with 450 mg of active material (synthesized/commercial $LaNi_5$) and 84 mg of a 60% PTFE emulsion in a mass ratio of $LaNi_5$:PTFE = 9:1. The mixture was manually ground with a pestle, followed by the addition of isopropanol to achieve a paste-like consistency. The paste was then rolled into a thin film (~10 μm thick), air-dried for 2–3 h, and further dried in a vacuum oven at 80 °C for 12 hours. The final electrodes were cut to a diameter of 7 mm.

2.5 Characterization Methods

The synthesized powders were analyzed using X-ray diffraction (XRD) on a TD-3700 diffractometer (Tongda, China) equipped with a copper radiation source (λCuKα1 = 1.54056 Å and λCuKα2 = 1.54439 Å).

Particle size distribution was determined using laser diffraction analysis on a HORIBA LA-960 particle size analyzer (Japan).

The morphology of the $LaNi_5$ particles was examined by scanning electron microscopy (SEM) using a Quanta 3D 200i Dual system microscope (FEI, USA).

Electrochemical measurements were performed using electrochemical impedance spectroscopy (EIS), cyclic voltammetry (CV), and galvanostatic cycling with a Biologic SP-300 potentiostat-galvanostat. All electrochemical experiments were conducted using a Swagelok-type three-electrode cell, with a carbon cloth counter electrode (SCF180H, China), a mercury/mercuric oxide (Hg/HgO) reference electrode, and a 6 M KOH electrolyte.

Cyclic voltammetry was carried out at a scan rate of 1 mV/s, while galvanostatic charge/discharge cycling was performed at a 0.5C rate within a voltage range of -1.2 V to 0.4 V (vs Hg/HgO). Electrochemical impedance spectra were recorded over a frequency range of 0.1 Hz to 7 MHz with an input signal amplitude of 10 mV.

3. Results and Discussion

Following the synthesis and preparation of $LaNi_5$ intermetallic, a series of studies were conducted to determine its phase composition, morphology, particle size distribution, and electrochemical characteristics.

The phase composition of the obtained product was analyzed by X-ray diffraction analysis. The diffractogram (Fig. 1, green curve) shows a set of reflexes characteristic for $LaNi_5$ intermetallide crystallizing in hexagonal structure (space group P6/mmm).

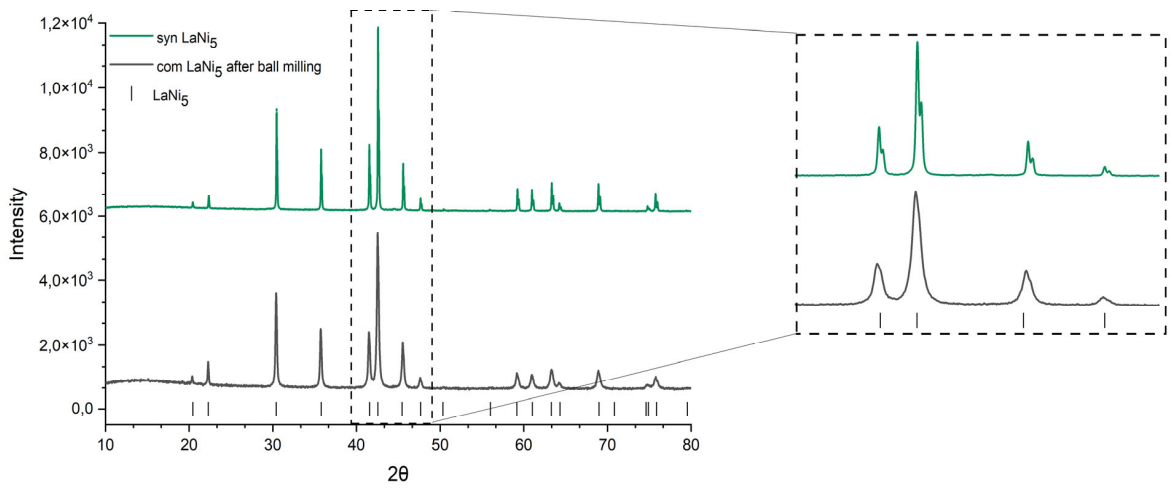

Fig. 1. Diffractograms of synthesized (green) and commercial, after grinding (black) $LaNi_5$.

The refined unit cell parameters (a = 5.019(4) Å, c = 3.978(2) Å, V = 86.826(6) Å^3) agree well with the literature data [23] (a = 5.013 Å, c = 3.987 Å, V = 86.77 Å^3). No impurities were detected, which indicates the complete conversion of oxide phases into the target intermetallic phase $LaNi_5$.

To evaluate the electrochemical characteristics of the synthesized material, a comparison was made with a commercial $LaNi_5$ sample, which, according to the manufacturer, has a coarse particle size distribution (approximately 100 µm). Since particles of this size make electrode formation difficult, the powder was subjected to mechanical grinding in a ball mill.

To ensure that the mechanical treatment did not disrupt the crystalline structure of the intermetallic compound, the commercial $LaNi_5$ after grinding was also analyzed using X-ray diffraction (Fig. 1, black curve). The positions of the main reflections remained unchanged, indicating the absence of phase transformations and the preservation of the structure. At the same time, a significant broadening of the peaks was observed, which, in this case, cannot be directly attributed to a reduction in the average crystallite size, as ball milling produces powder in the micron range. Most likely, this broadening is due to the accumulation of structural defects (microstrains, dislocations) arising from mechanical impact during grinding.

To assess the morphology and particle sizes of the obtained samples, both $LaNi_5$ samples (synthesized and commercial after grinding) were examined using complementary methods: scanning electron microscopy (SEM) and laser diffraction analysis (Fig. 2). According to SEM data, the synthesized material consists of particles with lengths ranging from 300 to 700 nm, whereas the commercial sample contains larger particles, mostly in the range of 1–5 µm. In both cases, the particles tend to form aggregates.

Laser diffraction analysis (Fig. 2 b, d) showed that both the synthesized and commercial powders have an unimodal size distribution. However, the peak values for the synthesized sample (about 5.9 µm) and the commercial one (approximately 8.4 µm) were significantly higher than the values obtained from SEM. This discrepancy is explained by the fact that laser analysis detects already-formed agglomerates of primary particles.

After the physicochemical studies were conducted, electrodes were fabricated from both the synthesized and commercial $LaNi_5$ samples using the method described in the experimental section.

To analyze the kinetics of the electrode processes and investigate the electrochemical reversibility of hydrogen sorption/desorption reactions, cyclic voltammetry was used. The cyclic voltammograms of the second cycle, presented in Fig. 3, demonstrate differences in the electrochemical behavior of the synthesized (solid black line) and commercial (dashed green line) $LaNi_5$ samples. In the region of negative potentials, both samples exhibit cathodic loops of the anodic peak, corresponding to the processes of hydrogen adsorption and desorption [24,25].

However, the synthesized $LaNi_5$ is characterized by sharper and narrower peaks (in both the cathodic and anodic regions), whereas the peaks of the commercial sample are noticeably broader and accompanied by lower current densities. The "sharper" peaks of the synthesized material indicate reduced resistance to the electrochemical process, which suggests improved kinetic characteristics and enhanced reversibility of hydrogen sorption/desorption reactions.

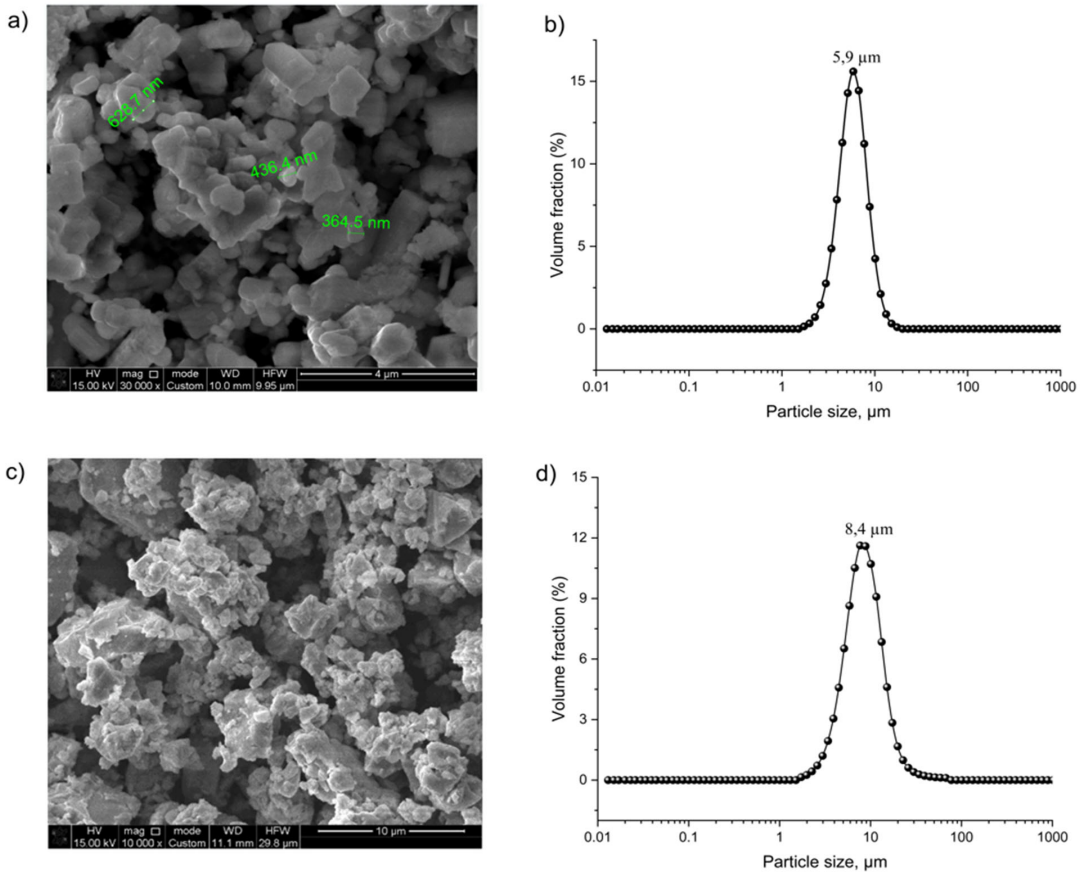

Fig. 2. SEM images and particle size distributions of $LaNi_5$: (a, b) synthesized; (c, d) commercial (after grinding).

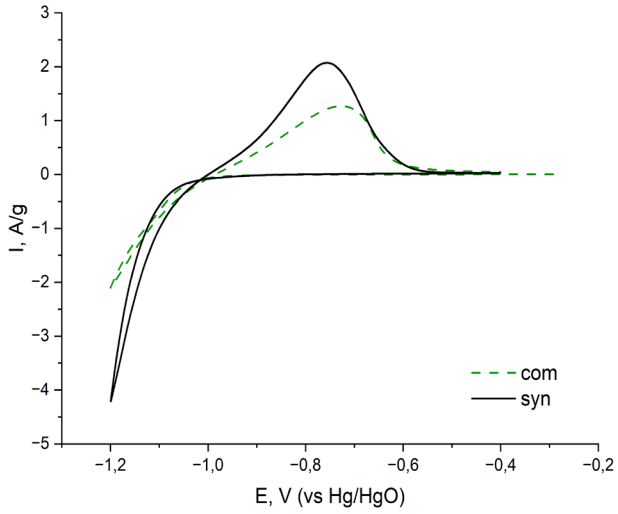

Fig. 3. Cyclic voltammograms of the second cycle for commercial (green, dashed) and synthesized (solid black) $LaNi_5$ at a scan rate of 1 mV/s.

These differences may be attributed to structural features: despite the similar agglomerate sizes (approximately 5 µm for the synthesized material and 9 µm for the commercial material after mechanical grinding), the synthesized $LaNi_5$ consists of nanoparticles, whereas the commercial material is formed from fragmented larger pieces. It is assumed that the presence of nanosized primary particles provides an increased specific surface area, facilitates contact with the electrolyte, and promotes accelerated transport and diffusion of hydrogen within the active material.

To gain a more detailed understanding of the resistance of electrochemical processes and to determine the nature of the differences in the behavior of the synthesized and commercial samples, the electrodes were polarized to -1 V (charged state) and subjected to cyclic impedance spectroscopy. The obtained impedance spectra were refined using an electrical circuit model consisting of sequentially connected elements and their groups: an inductance (L1) and a resistor (R1) (representing the contribution of wires and electrolyte), a parallel combination of a constant phase element (Q1) and a resistor (R2) (accounting for the intergranular resistance of agglomerates), another parallel combination of a constant phase element (Q2) and a resistor (R3) (representing the intragranular resistance of individual particles), and a constant phase element (Q3) (contributing to electrode blocking and partially to ion diffusion in solution) (Fig. 4c). For both samples,

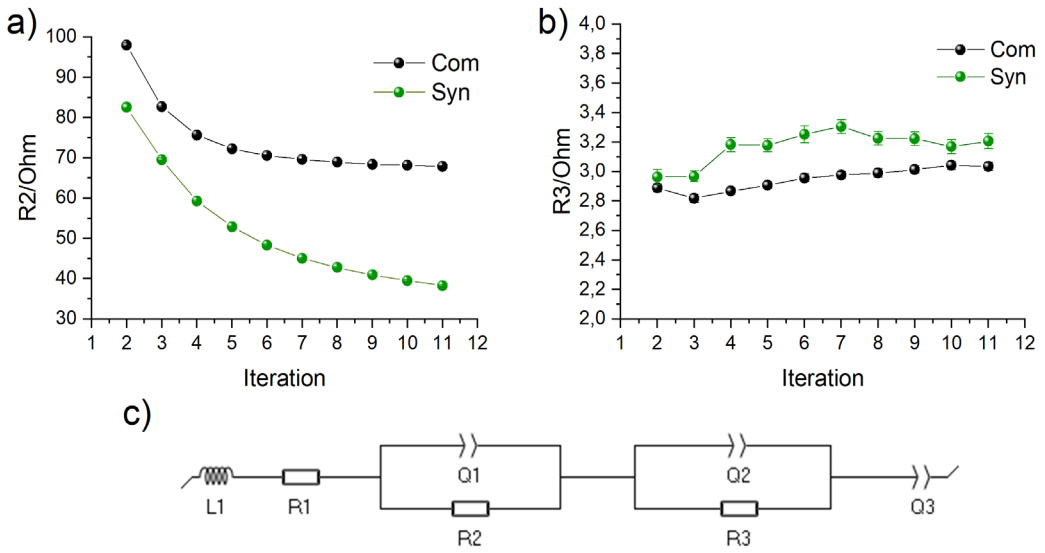

Fig. 4. Resistance of equivalent elements in the electrical circuit model obtained from impedance spectroscopy data: (a) contribution of intergranular resistance of agglomerates; (b) contribution of intragranular resistance of individual particles; (c) equivalent electrical circuit.

the contribution of the electrolyte and wires (R1) to the total resistance remained constant at approximately 2 Ω, which is expected for the electrolyte. It is also worth noting that the intragranular resistance – ion migration within the material particles – was nearly identical (~3 Ω), confirming the structural similarity and comparable properties of the investigated samples (Fig. 4b). However, the intergranular resistance of agglomerates in the synthesized sample decreased more significantly over multiple impedance spectra cycles (by approximately a factor of 2 over 10 iterations) compared to the commercial sample (by about 1.5 times over 10 iterations) (Fig. 4a).

It can be assumed that when an alternating current is applied to the electrodes, some form of material activation occurs, enabling more efficient ion transport between agglomerates. Given the smaller particle size of the synthesized sample, it is likely that cracking occurs more effectively, thereby increasing the active surface area and reducing the overall system resistance. This observation is in good agreement with the cyclic voltammetry data.

The electrochemical stability and specific capacity were evaluated using galvanostatic cycling. Figure 5 presents the capacity evolution over time for the synthesized (black curve) and commercial (green curve) $LaNi_5$ samples. During prolonged cycling, both samples undergo an activation stage, but in different ways.

The commercial $LaNi_5$ starts with a relatively low specific capacity (~110 mAh/g), which gradually increases to ~190 mAh/g by the 30th cycle, then stabilizes around 185 mAh/g. This smooth increase is likely due to the gradual fragmentation of large particles, the breakdown of surface oxide layers, and the formation of microcracks, leading to an increased accessible surface area and improved hydrogen diffusion conditions within the material.

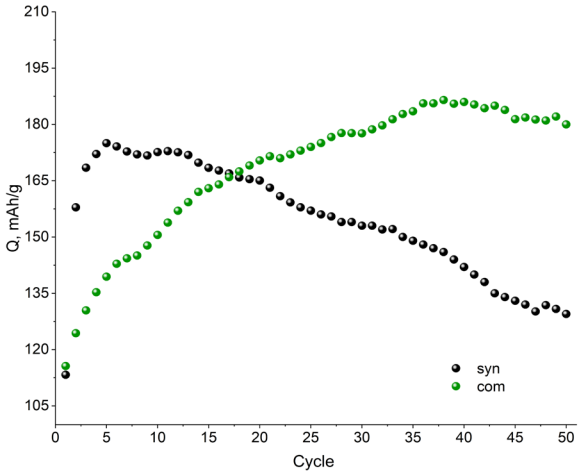

Fig. 5. 50 charge/discharge cycles for commercial (green) and synthesized (black) $LaNi_5$.

The synthesized $LaNi_5$ also undergoes an activation stage, but it progresses much faster: by the fifth cycle, its specific capacity reaches ~180 mAh/g, starting from 114 mAh/g in the first cycle. However, a gradual degradation follows, and by the 50th cycle, the capacity decreases to 130 mAh/g.

The observed capacity fade of the synthesized nano-$LaNi_5$ during prolonged cycling (Fig. 5), decreasing to 130 mAh/g by the 50th cycle, is consistent with the findings of Liu et al. [23] for similar nanostructured materials. Although nanostructuring enhances the initial kinetics, the high density of intergranular boundaries and the increased specific surface area seem to accelerate degradation processes. Repeated lattice volume changes during cycling concentrate mechanical stress at the grain boundaries, facilitating the generation of internal defects. These defects are predominantly newly formed during cycling due to the repeated stress. This is supported by data from Liu et al. [23], who recorded a significant decrease in crystallite size and the formation of lattice defects within $LaNi_5$ nanoparticles after cycling, even while the overall particle morphology remained stable. Simultaneously, the large surface area increases the material susceptibility to passivation or corrosion in the electrolyte. The accumulation of this surface and internal damage over time leads to particle pulverization, loss of electrical contact, and consequently, to lower long-term stability compared to the microcrystalline commercial sample. Thus, a critical trade-off between enhanced kinetics and reduced cyclability becomes apparent for the nanostructured anodes.

4. Conclusion

This study presents a comparative investigation of the electrochemical properties of nanostructured $LaNi_5$ intermetallic, synthesized via the sol-gel method, and its commercial counterpart, produced by traditional fusion followed by mechanical grinding, for application as an anode material in Ni-MH batteries. It was established that the synthesized material, consisting of primary nanoparticles ranging from 300 to 700 nm that form agglomerates of about 5.9 µm, exhibits significantly improved kinetic characteristics compared to the commercial microcrystalline sample (agglomerates ~8.4 µm), including lower polarization resistance and more efficient mass transport. The synthesized $LaNi_5$ activates rapidly, reaching a maximum capacity of ~180 mAh/g by the 5th cycle. However, upon prolonged cycling, it exhibited lower stability, with the capacity decreasing to 130 mAh/g by the 50th cycle, in contrast to the commercial sample, whose capacity gradually increased to ~190 mAh/g and then stabilized. This observed trade-off between the enhanced kinetic properties and the reduced cyclability of the nanostructured $LaNi_5$ highlights important aspects for the further optimization of anode materials based on this intermetallic compound.

Acknowledgments

This research is funded by the Ministry of Science and Higher Education of the Republic of Kazakhstan (Grant No. BR21882200)

References

[1]. N.C. Alluraiah, V. Nandagopal, P. Veeramanikandan, G. D, S. Meena, G. Brindha. Comparison of SoC in Ni-MH and Lithium-Ion Battery for E-Vehicle. *Int. J. Electr. Electron. Res*. 12 (2024) 1258–1263. DOI: 10.37391/ijeer.120417

[2]. M. Tliha, C. Khaldi, S. Boussami, N. Fenineche, O. El-Kedim, H. Mathlouthi, J. Lamloumi. Kinetic and thermodynamic studies of hydrogen storage alloys as negative electrode materials for Ni/MH batteries: a review. *J. Solid State Electrochem.* 18 (2014) 577–593. DOI: 10.1007/s10008-013-2300-3

[3]. L. Ouyang, J. Huang, H. Wang, J. Liu, M. Zhu. Progress of hydrogen storage alloys for Ni-MH rechargeable power batteries in electric vehicles: A review. *Mater. Chem. Phys*. 200 (2017)164–178. DOI: 10.1016/j.matchemphys.2017.07.002

[4]. S. Abdimomyn, S. Malik, M. Skakov, Y. Koyanbayev, A. Miniyazov, F. Malchik. Hydrogen Storage Materials: Promising Materials for Kazakhstan's Hydrogen Storage Industry. *Eurasian Chem.-Technol. J.* 26 (2024) 113–132. DOI: 10.18321/ectj1635

[5]. L. Schlapbach, A. Züttel. Hydrogen-storage materials for mobile applications. *Nature* 414 (2001) 353–358. DOI: 10.1038/35104634

[6]. G. Sandrock. A panoramic overview of hydrogen storage alloys from a gas reaction point of view. *J. Alloys Compd.* 293-295 (1999) 877–888. DOI: 10.1016/S0925-8388(99)00384-9

[7]. R. Sarhaddi, H. Arabi, F. Pourarian. Structural, morphological, magnetic and hydrogen absorption properties of $LaNi_5$ alloy: A comprehensive study. *Int. J. Mod. Phys. B* 28 (2014) 1450079. DOI: 10.1142/S0217979214500799

[8]. S. Srivastava, S.S.S. Raman, B.K. Singh, O.N. Srivastava. On the synthesis and characterization of some new AB_5 type $MmNi_{4.3}Al_{0.3}Mn_{0.4}$, $LaNi_{5-x}Si_x$ (x=0.1, 0.3, 0.5) and Mg−x wt% $CFMmNi_{5-y}$ wt% Si hydrogen storage materials. *Int. J. Hydrogen Energy* 25 (2000) 431–440. DOI: 10.1016/S0360-3199(99)00055-5

[9]. M.H. Enayati, F.A. Mohamed. Application of mechanical alloying/milling for synthesis of nanocrystalline and amorphous materials. *Int. Mater. Rev.* 59 (2014) 394–416. DOI: 10.1179/1743280414Y.0000000036

[10]. L. Wei, S. Abd Rahim, M. Al Bakri Abdullah, A. Yin, M. Ghazali, M. Omar, O. Nemeș, A. Sandu, P. Vizureanu, A. Abdellah. Producing Metal Powder from Machining Chips Using Ball Milling Process: A Review. *Materials* 16 (2023) 4635. DOI: 10.3390/ma16134635

[11]. J. Kusiński, K. Kowalski, S. Kac, P. Matteazzi, M. Krebs, J. Morgiel, S. Cochet. Microstructure of LaNi5 Base Nanopowders Produced by High Energy Ball Milling. *Solid State Phenomena* 186 (2012) 124–129. DOI: 10.4028/www.scientific.net/SSP.186.124

[12]. B. Joseph, B. Schiavo, G. D'Alì Staiti, B.R. Sekhar. An experimental investigation on the poor hydrogen sorption properties of nanostructured $LaNi_5$ prepared by ball-milling. *Int. J. Hydrogen Energy* 36 (2011) 7914–7919. DOI: 10.1016/j.ijhydene.2011.01.090

[13]. B.A. Talagañis, M.R. Esquivel, G. Meyer. Improvement of as-milled properties of mechanically alloyed $LaNi_5$ and application to hydrogen thermal compression. *Int. J. Hydrogen Energy* 36 (2011) 11961–11968. DOI: 10.1016/j.ijhydene.2011.06.047

[14]. A. Bishnoi, S. Pati, P. Sharma. Architectural design of metal hydrides to improve the hydro-gen storage characteristics. *J. Power Sources* 608 (2024) 234609. DOI: 10.1016/j.jpowsour.2024.234609

[15]. M. Ji, X. Tian, X. Liu, J. Yan, Y. Zhang, R. Guo, W. Wei, Y. Yang. The catalytic oxidation properties for BH_4^- and electrochemical properties of the Ag-decorated AB_5-type hydrogen storage alloy. *J. Phys. Chem. Solids* 166 (2022) 110709. DOI: 10.1016/j.jpcs.2022.110709

[16]. J. Liu, K. Li, H. Cheng, K. Yan, Y. Wang, Y. Liu, H. Jin, Z. Zheng. New insights into the hydrogen storage performance degradation and Al functioning mechanism of $LaNi_5$-Al alloys. *Int. J. Hydrogen Energy* 42 (2017) 24904–24914. DOI: 10.1016/j.ijhydene.2017.07.213

[17]. H. Ahn, J. Lee. Intrinsic degradation of $LaNi_5$ by the temperature induced hydrogen absorption-desorption cycling. *Int. J. Hydrogen Energy* 16 (1991) 93–99. DOI: 10.1016/0360-3199(91)90035-H

[18]. T. Liu, C. Chen, C. Qin, X. Li. Improved hydrogen storage properties of Mg-based nanocomposite by addition of $LaNi_5$ nanoparticles. *Int. J. Hydrogen Energy* 39 (2014) 18273–18279. DOI: 10.1016/j.ijhydene.2014.03.041

[19]. F. Chiesa, M. Rigaud. La réduction de l'oxyde de nickel par l'hydrogène. *Can. J. Chem. Eng*. 49 (1971) 617–620. https://doi.org/10.1002/cjce.5450490511

[20]. N. Yasuda, T. Tsuchiya, S. Sasaki, N. Okinaka, T. Akiyama. Self-ignition combustion synthesis of $LaNi_5$ at different hydrogen pressures. *Int. J. Hydrogen Energy* 36 (2011) 8604–8609. DOi: 10.1016/j.ijhydene.2011.04.017

[21]. L.J. Bannenberg, B. Boshuizen, F.A. Ardy Nugroho, H. Schreuders. Hydrogenation kinetics of metal hydride catalytic layers. *ACS Appl. Mater. Interfaces* 13 (2021) 52530–52541. DOI: 10.1021/acsami.1c13240

[22]. A.G. Burlakova, S.P. Shilkin. Reaction of lanthanum carbonates with nickel in aqueous medium. *Russ. J. Gen. Chem.* 73 (2003) 1331–1334. DOI: 10.1023/B:RUGC.0000015971.66514.8f

[23]. W. Liu, K.-F. Aguey-Zinsou. Low temperature synthesis of $LaNi_5$ nanoparticles for hydrogen storage. *Int. J. Hydrogen Energy* 41 (2016) 1679–1687. DOI: 10.1016/j.ijhydene.2015.10.128

[24]. J. Han, Electrochemical properties of metal hydride electrodes. Doctoral Thesis, 2000. https://scholar.uwindsor.ca/etd/1897/

[25]. M. Dymek, H. Bala. Hydrogen diffusivity in the massive $LaNi_5$ electrode using voltammetry technique. *J. Solid State Electrochem*. 18(11) (2014) 3033–3037. DOI: 10.1007/s10008-013-2339-1